J Geophys (1984) 56: 24–33

Journal of Geophysics

The relaxation of spherical and flat Maxwell Earth models and effects due to the presence of the lithosphere

Detlef Wolf
Department of Physics, University of Toronto, Toronto, Ontario, Canada, M5S 1A7

Abstract. The radial surface deflection of a spherical Earth model appropriate to time scales characteristic of glacial loading is compared with the associated half-space response. For that purpose the analytical solution for a Maxwell sphere surrounded by a thick elastic shell is derived under the assumption of incompressibility. The half-space approximation is deduced as a special case directly from the spherical solution. Comparison of the response spectra, for different thicknesses of the elastic shell, reveals only minor differences. In the spatial domain, the half-space approximation may, nevertheless, diverge significantly from the spherical solution. For a disk load radius $R = 800$ km (Fennoscandia), the half-space approximation is adequate, whereas it is usually inappropriate if $R = 1600$ km (Laurentia). The sensitivity of the response to the thickness of the elastic shell is also investigated. For $R = 800$ km, the surface deflection in the central region below the load is fairly diagnostic of the shell thickness. If $R = 1600$ km, the peripheral region is more sensitive to this parameter.

Key Words: Isostasy – Lithosphere – Maxwell continuum

Introduction

The isostatic adjustment of the Earth due to viscous flow in its mantle is a problem on which work has continued for nearly 50 years. The main results have been reviewed by Cathles (1975), Peltier (1982) and others. The effect of the lithosphere on the response characteristics has, however, been fully appreciated only during the past few years. Earlier work was inconclusive in this respect. This is exemplified by two interpretations of strandline data from the region of Pleistocene Lake Bonneville in the United States. Whereas Crittenden (1963) neglected the lithosphere and inferred a mantle viscosity of 10^{21} P from the data, Walcott (1970a) treated the mantle as inviscid and derived a value of 5×10^{22} Nm for the flexural rigidity of the lithosphere. Later, Nakiboglu and Lambeck (1982) re-interpreted the data, using an improved viscoelastic model incorporating both a lithosphere *and* a dynamic mantle, and suggested revised values for lithospheric thickness and mantle viscosity.

The modification of the response pattern of Maxwell Earth models by the presence of the lithosphere has been addressed by Peltier (1980) and by Wu and Peltier (1982). The analysis has recently been extended such that lithospheric thickness can be directly inferred from appropriate isostatic adjustment data (Peltier, 1984).

In the present investigation, the effect of the lithosphere on the response of Maxwell Earth models is analysed in greater detail. For this purpose straight-edged circular loads of radii $R = 800$ km (Fennoscandia) or $R = 1600$ km (Laurentia) are applied at times $t \geqq 0$, and the relaxation of the surface is investigated. For loads comparable in scale to the larger disk, the sensitivity of the deflection in the peripheral region of the load to lithospheric thickness has already been demonstrated by Peltier (1984) in his analysis of relative-sea-level variations induced by the melting of the Laurentide ice sheet in Canada.

The smaller disk load may serve as a crude representation of the Fennoscandian ice sheet. On this load scale the significance of the lithosphere has been less clear. Cathles (1975, pp. 144–155) discussed the controversy and concluded that the effect of the lithosphere could be neglected when modelling the Fennoscandian uplift. His reasoning was, however, primarily based on the analysis of the wave-number spectrum of the load. Here we will study the effects of the lithosphere in the spatial domain. As will be shown, the shape of the deformed surface in the region formerly covered by the Fennoscandian ice load is quite sensitive to the presence of the lithosphere and may therefore be used to infer its thickness.

A second aspect of our analysis concerns the adequacy of flat-earth approximations when modelling the response due to loads of large diameter. Whereas half-space models are conventional for small loads such as lakes or volcanic islands, some uncertainty exists about the maximum load diameter tolerable in this approximation. The deglaciation-induced uplift of Fennoscandia, for example, has been modelled using both spherical and half-space theory (see Cathles, 1975, pp. 6, 173–180, for a review). The Laurentide ice load, on the other hand, has usually been regarded as too large for the application of flat-earth approximations (see Peltier, 1982).

All models to be discussed in the present study

apply to externally gravitating, incompressible and hydrostatically pre-stressed continua of uniform density. Thus, the gravitational effects disregarded in our models reduce to perturbations of the geopotential due to (a) the externally applied force field, viz. the "load", and (b) due to internal mass redistributions induced by this load.

Cathles (1975, pp. 72–83) has presented solutions for the surface deformation of elastic Earth models of increasing complexity and discussed the contributions of different gravitational effects. This also includes an assessment of the influence of the inviscid core on the observed response. From his study it can be inferred that the significance of the geometrical and gravitational effects of spherical Earth models is mainly confined to angular orders $n<10$. As Cathles further shows, contributions (a) and (b) to the perturbation of the geopotential largely cancel each other, such that the net effect of self-gravitation is small. The influence of the Earth's core becomes perceptible at angular orders $n<5$. The error committed when neglecting both self-gravitation and the core in the spherical solution amounts to 5–10 per cent of the surface deflection. For $n<5$ this is smaller, by a factor of more than two, than the purely geometrical effect of sphericity.

The significance of self-gravitation for the relaxation of spherical Maxwell Earth models is not very well documented. As a crude guideline, strains in the elastic problem translate into strain rates in the associated viscoelastic problem. Therefore, changes in the deformation of an elastic sphere due to self-gravitation and the inviscid core are paralleled by corresponding changes in the relaxation times of a Maxwell sphere. As relaxation proceeds, the Maxwell continuum degenerates into an inviscid fluid, and the core loses its special role. Quantitative studies are, however, lacking so far. Recently, Dragoni et al. (1983) have derived analytical solutions for the deformation of a two-layer incompressible Maxwell sphere without a core in an attempt to examine whether earthquake-triggered movements of material can excite the Chandler wobble. The inclusion of self-gravitation into their analysis is reflected by the great complexity of their equations. If desired, appropriate modifications of their solution would permit a quantitative assessment of the effects of self-gravitation on the relaxation of spherical Maxwell Earth models.

In view of the limited objectives of the present study, the neglect of both self-gravitation and the inviscid core appears to be justified. In the following we will therefore derive the analytical solution describing the deformation of a two-layered, incompressible and pre-stressed Maxwell Earth model subject to an external gravity field and deduce the half-space limit directly from this solution. This approach will then allow us to obtain better constraints on the range of load scales amenable to flat-earth approximations.

Theory

Our derivation of the equations appropriate to the quasi-static deformation of a Maxwell sphere will be based on the correspondence principle. For geophysical applications, this method has been developed in papers that began with Peltier (1974). Major results from this work are summarized in Peltier (1982). The main advantage of the correspondence principle is that it allows us to derive the viscoelastic solution from the solution for an associated elastic problem. For the present purpose it is sufficient to restrict our analysis to incompressible Earth models. Together with the assumption of external gravitation this significantly simplifies the general form of the momentum balance appropriate to the quasi-static deformation of a viscoelastic continuum (Peltier, 1974). Defining a total perturbation stress by

$$\sigma_{ij}=\sigma_{ij}^{(e)}-\rho\, g\, u_r \frac{r}{a_1}\delta_{ij}, \tag{1}$$

the momentum balance in Cartesian co-ordinates x_i is

$$\frac{\partial}{\partial x_j}\sigma_{ij}=0. \tag{2}$$

In Eq. (1) $\sigma_{ij}^{(e)}$ denotes the elastic portion of the perturbation stress, and $\rho\, g\, u_r(r/a_1)\,\delta_{ij}$ accounts for stress advection in a hydrostatically pre-stressed sphere of radius a_1 and density ρ subject to gravitational acceleration g, with u_r the radial displacement component at the radial distance r (Love, 1911, pp. 89–93). The pre-stress term was first included in the viscoelastic formulation by Peltier (1974). Its importance was explicitly discussed by Wu and Peltier (1982), who noted that its consideration in the momentum balance is required in order that, for a Heaviside loading history, the correct solution be obtained in the inviscid limit ($t\to\infty$) of the viscoelastic continuum. Recently, the significance of pre-stress has been further analysed by Wolf (1984a).

Since incompressibility has been assumed, Hooke's law takes the form

$$\sigma_{ij}^{(e)}=-p^{(e)}\,\delta_{ij}+\mu\left(\frac{\partial u_i}{\partial x_j}+\frac{\partial u_j}{\partial x_i}\right), \tag{3}$$

with μ Lame's second constant and u_i the displacement. $p^{(e)}$ denotes the elastic portion of the perturbation pressure p and

$$p^{(e)}=\lim_{\substack{\lambda\to\infty\\ \Delta\to 0}}(\lambda\Delta), \tag{4}$$

where λ is Lame's first constant, and $\Delta=\partial u_i/\partial x_i$ denotes the dilatation (Love, 1927, pp. 255–257). Substituting for σ_{ij} in Eq. (2) yields

$$-\frac{\partial p}{\partial x_j}\delta_{ij}+\mu\frac{\partial^2 u_i}{\partial x_j^2}=0, \tag{5a}$$

or, in vector notation,

$$-\nabla p-\mu\nabla\times\nabla\times\mathbf{u}=0. \tag{5b}$$

Confining our analysis to axially symmetric problems, we obtain for the radial and zonal components of Eq. (5b), respectively

$$\frac{\partial}{\partial\theta}(2r\,\omega_\phi\sin\theta)+r^2\,\mu^{-1}\sin\theta\frac{\partial p}{\partial r}=0, \tag{6}$$

$$\frac{\partial}{\partial r}(2r\omega_\phi)-\mu^{-1}\frac{\partial p}{\partial\theta}=0, \tag{7}$$

where $2\omega_\phi=(\nabla\times\mathbf{u})_\phi$ is implied. Here r, θ and ϕ denote the radial, zonal and azimuthal components of the co-ordinate vector, respectively, with $\theta=0$ on the axis of symmetry. For spherical co-ordinates, the equation of continuity $\nabla\cdot\mathbf{u}=0$ becomes

$$\sin\theta\frac{\partial}{\partial r}(r^2u_r)+r\frac{\partial}{\partial\theta}(u_\theta\sin\theta)=0. \tag{8}$$

To solve the system of Eqs. (6)-(8) for u_r, u_θ and p, we seek solutions of the type

$$u_r=R_1(r)P_n(\cos\theta), \tag{9}$$

$$u_\theta=-R_2(r)\sin\theta P_n'(\cos\theta), \tag{10}$$

$$p=R_3(r)P_n(\cos\theta). \tag{11}$$

Here P_n is the Legendre polynomial of degree n, where $n=0,1,\ldots$, and a prime denotes differentiation with respect to the argument. Substitution in Eqs. (6)-(8) yields

$$n(n+1)(R_1-rR_2'-R_2)+\mu^{-1}r^2R_3'=0, \tag{12}$$

$$R_1'-2R_2'-rR_2''+\mu^{-1}R_3=0, \tag{13}$$

$$rR_1'+2R_1-n(n+1)R_2=0. \tag{14}$$

Equations (12)-(14) constitute a system of coupled ordinary differential equations for R_1, R_2 and R_3. Eliminating R_2 and R_3 in Eqs. (12) and (13) yields

$$r^4R_1^{(4)}+8r^3R_1^{(3)}+2[6-n(n+1)]r^2R_1''-4n(n+1)rR_1'$$
$$-n(n+1)[2-n(n+1)]R_1=0. \tag{15}$$

The solution of Eq. (15) is

$$R_1=A_nr^{n+1}+B_nr^{-n}+C_nr^{n-1}+D_nr^{-(n+2)}. \tag{16}$$

Substituting for R_1 and R_1' in Eq. (14) we obtain

$$R_2=\frac{1}{n(n+1)}[(n+3)A_nr^{n+1}-(n-2)B_nr^{-n}$$
$$+(n+1)C_nr^{n-1}-nD_nr^{-(n+2)}]. \tag{17}$$

Solving Eqs. (12) and (13) for R_3 yields

$$r^2R_3''+2rR_3'-n(n+1)R_3=0, \tag{18}$$

with the solution

$$R_3=E_nr^n+F_nr^{-(n+1)}. \tag{19}$$

The integration constants E_n and F_n are not independent. Substituting in Eq. (12) and equating coefficients we obtain

$$nE_n=2\mu(2n+3)A_n, \tag{20}$$

$$(n+1)F_n=2\mu(2n-1)B_n. \tag{21}$$

For the elastic shell, where $\mu=\mu_1$, the solutions for displacement components and pressure are therefore of the type

$$u_r(r,\theta)=[A_nr^{n+1}+B_nr^{-n}+C_nr^{n-1}+D_nr^{-(n+2)}]P_n(\cos\theta), \tag{22}$$

$$u_\theta(r,\theta)=-\frac{1}{n(n+1)}[(n+3)A_nr^{n+1}-(n-2)B_nr^{-n}$$
$$+(n+1)C_nr^{n-1}-nD_nr^{-(n+2)}]\sin\theta P_n'(\cos\theta), \tag{23}$$

$$p(r,\theta)=2\mu_1\left[\frac{2n+3}{n}A_nr^n+\frac{2n-1}{n+1}B_nr^{-(n+1)}\right]P_n(\cos\theta). \tag{24}$$

If we observe that

$$\sigma_{rr}=-p+2\mu_1\frac{\partial u_r}{\partial r}, \tag{25}$$

$$r\sigma_{r\theta}=\mu_1\left(\frac{\partial u_r}{\partial\theta}-u_\theta+r\frac{\partial u_\theta}{\partial r}\right), \tag{26}$$

the solutions for the stress components can be shown to be of the type

$$\sigma_{rr}(r,\theta)=2\mu_1\left[\frac{n^2-n-3}{n}A_nr^n-\frac{n^2+3n-1}{n+1}B_nr^{-(n+1)}\right.$$
$$\left.+(n-1)C_nr^{n-2}-(n+2)D_nr^{-(n+3)}\right]P_n(\cos\theta), \tag{27}$$

$$\sigma_{r\theta}(r,\theta)=-\frac{2\mu_1}{n(n+1)}[n(n+2)A_nr^n+(n^2-1)B_nr^{-(n+1)}$$
$$+(n^2-1)C_nr^{n-2}+n(n+2)D_nr^{-(n+3)}]\sin\theta P_n'(\cos\theta). \tag{28}$$

The integration constants A_n, B_n, C_n and D_n can be determined from the boundary conditions. If the elastic sphere is subject to a load pressure P_n, we have for the elastic perturbation stress at the surface $r=a_1$

$$\sigma_{rr}^{(e)}(a_1,\theta)=-P_n(\cos\theta), \tag{29}$$

$$\sigma_{r\theta}^{(e)}(a_1,\theta)=0. \tag{30}$$

From the general solution for the deformation of a uniform elastic sphere of rigidity μ_2, we obtain at the interface $r=a_2$ between mantle and shell (see Appendix A),

$$2\mu_2(n-1)(2n^2+4n+3)u_r(a_2,\theta)$$
$$=na_2\left[(2n+1)\sigma_{rr}(a_2,\theta)-3(n+1)\frac{P_n}{\sin\theta P_n'}\sigma_{r\theta}(a_2,\theta)\right], \tag{31}$$

$$2\mu_2(n-1)(2n^2+4n+3)u_\theta(a_2,\theta)$$
$$=-a_2\left[3\frac{\sin\theta P_n'}{P_n}\sigma_{rr}(a_2,\theta)-(2n^2+n+3)\sigma_{r\theta}(a_2,\theta)\right]. \tag{32}$$

Substituting in Eqs. (29)-(32) for u_r, u_θ, σ_{rr} and $\sigma_{r\theta}$ from Eqs. (22), (23), (27) and (28) at $r=a_2$, a system of four equations is obtained, which allows the determination of the four integration constants for the specified boundary conditions. After considerable algebraic manipulation we obtain

$$A_n=-\frac{n(n+1)(n^2-1)}{2\mu_1D}[k_1-k_2(a_2/a_1)^{-2}$$
$$+k_3(a_2/a_1)^{-(2n+1)}], \tag{33}$$

$$B_n=\frac{n^2(n+1)(n+2)}{2\mu_1D}[k_4-k_2(a_2/a_1)^{-2}$$
$$+k_5(a_2/a_1)^{2n+1}], \tag{34}$$

$$C_n=-\frac{n^2(n+1)(n+2)}{2\mu_1D}[k_4-k_6(a_2/a_1)^2-k_3(a_2/a_1)^{-(2n+1)}], \tag{35}$$

$$D_n=\frac{n(n+1)(n^2-1)}{2\mu_1D}[k_1-k_6(a_2/a_1)^2-k_5(a_2/a_1)^{2n+1}]. \tag{36}$$

Here the integration constants have been transformed according to $a_1^n A_n \to A_n$, $a_1^{-(n+1)} B_n \to B_n$, $a_1^{n-2} C_n \to C_n$, $a_1^{-(n+3)} D_n \to D_n$. $k_1, \ldots, k_6$ and D are complicated expressions in terms of μ_1, μ_2, ρ and n (see Appendix B).

In the following we will be concerned with the radial surface displacement $u_r(a_1, \theta)$. Substituting for the integration constants in Eq. (22) and putting $r = a_1$ yields

$$u_r = T_n^{(e)} P_n, \tag{37}$$

where

$$T_n^{(e)} = \frac{n(n+1)(2n+1)a_1}{2\mu_1 D}[k_6(a_2/a_1)^2 - k_2(a_2/a_1)^{-2} + k_5(a_2/a_1)^{2n+1} + k_3(a_2/a_1)^{-(2n+1)}]. \tag{38}$$

Several special solutions may be derived from Eq. (37); for example, the solution for the elastic shell surrounding an inviscid mantle, which is obtained by taking $\mu_2 = 0$. A similar solution was previously discussed by Slichter and Caputo (1960). Solutions for the uniform elastic sphere result from $\mu_1 = \mu_2$, $a_2 = 0$ or $a_1 = a_2$.

In the present context it is of particular interest to compare Eq. (37) with the associated flat-earth solution for the same physical model. The two-layer elastic half-space can be treated as a separate boundary-value problem. More insight is gained, however, if Eq. (37) is reduced to the flat-earth solution. This approach will be employed in what follows.

If $h = a_1 - a_2$, we simply require that h/a_1 is a small quantity. Also n must be large enough that $k = n/a_1$ remains finite. If we observe that $a_2/a_1 = 1 - h/a_1$, put $n\theta = nr'/a_1 = kr'$ and substitute the asymptotic approximations for the constants in $T_n^{(e)}$, we obtain, after some algebra, the flat-earth approximation of Eq. (37) as

$$u_r(a_1) = -w(0) = -T^{(e)}(k) J_0(kr'), \tag{39}$$

where

$$T^{(e)}(k) = \left\{\rho g - 2\mu_1 k \frac{(M^2-1)(kh)^2 + [M\cosh(kh) + \sinh(kh)]^2}{(M^2-1)kh - [M\sinh(kh) + \cosh(kh)][M\cosh(kh) + \sinh(kh)]}\right\}^{-1}, \tag{40}$$

with $M = \mu_2/\mu_1$. Here we have used an asymptotic approximation for Legendre polynomials in terms of Bessel functions, viz. (e.g. Watson, 1944, p. 155)

$$\lim_{\substack{n\to\infty \\ \theta\to 0}} P_n(\cos\theta) = J_0(n\theta), \tag{41}$$

where J_0 is the Bessel function of the first kind and zeroth order. r' denotes the radial co-ordinate in the cylindrical system $z = a_1 - r$, $r' = \theta a_1$, and w is the vertical displacement in this system. For $M = 0$, the lower half-space becomes inviscid. If, on the other hand, $\mu_1 = \mu_2$, Eq. (39) is reduced to

$$w(0) = \frac{1}{\rho g + 2\mu_1 k} J_0(kr'). \tag{42}$$

This is the solution for the uniform (and incompressible) elastic half-space. If pre-stress is neglected, Eq. (42) reduces to $w(0) = J_0/(2\mu_1 k)$ (e.g. Sneddon, 1951, pp. 468–486; Jeffreys, 1976, pp. 265–267).

In the following, we will be concerned with circular load distributions q in the form of straight-edged (spherical) caps or (plane) disks. Thus, for the sphere,

$$q(\theta) = \begin{cases} 0, & 0 \leqq \theta < \beta \\ 1/2, & \theta = \beta \\ 1, & \beta < \theta \leqq \pi \end{cases}, \tag{43}$$

and for the half-space

$$q(r') = \begin{cases} 0, & 0 \leqq r' < R \\ 1/2, & r' = R \\ 1, & R < r' < \infty \end{cases}. \tag{44}$$

Here $\beta = R/a_1$ is the angular radius of the cap and R the radius of the disk. $q(\theta)$ can be expanded into a Legendre series

$$q(\theta) = \sum_{n=0}^{\infty} q_n P_n(\cos\theta), \tag{45}$$

where (e.g. Lebedev, 1972, pp. 68–69)

$$q_n = \begin{cases} (1 - \cos\beta)/2, & n = 0 \\ [P_{n-1}(\cos\beta) - P_{n+1}(\cos\beta)]/2, & n = 1, 2 \ldots \end{cases}. \tag{46}$$

Similarly $q(r')$ can be written as the inverse zeroth-order Hankel transform, i.e.

$$q(r') = \int_0^{\infty} \hat{q}(k) k J_0(kr')\, dk, \tag{47}$$

where (e.g. Sneddon, 1951, p. 528)

$$\hat{q}(k) = \frac{R}{k} J_1(kR). \tag{48}$$

The generalization of our solutions for Maxwell continua is straightforward. Here we will only remark that the correspondence principle allows us to identify the solution of any elastic problem with the Laplace transform of the solution of an associated Maxwell problem, if we substitute

$$\lambda(s) = (\lambda s + \tau^{-1} K)/(s + \tau^{-1}), \tag{49}$$

$$\mu(s) = \mu s/(s + \tau^{-1}), \tag{50}$$

for λ and μ, respectively. In Eqs. (49) and (50) $\tau = \eta/\mu$, where η is the dynamic viscosity, $K = \lambda + 2/3\mu$ denotes the bulk modulus, and s is the Laplace transform variable of the time t.

Since the pronounced temperature dependence of viscosity renders most of the Earth's lithosphere elastic on a time scale of the order of 10 ka, $\eta_1 \to \infty$ and therefore $\mu_1(s) = \mu_1$, and the transformation only applies to μ_2.

Before the inverse Laplace transform can be implemented, some algebraic operations must be applied to the elastic solution. These are outlined in Appendix C.

Numerical Results

In order to illustrate the effects of sphericity, we begin with a comparison of the response spectra between the

spherical solution and those obtained in the half-space approximation. In the following, superscript e will refer to the amplitude of the elastic or instantaneous portion of the response, whereas superscript v will denote the viscous or time-dependent part of the response. We have, from Appendix C, for the viscoelastic transfer function $T^{(ve)}(t)$ of the continuum subject to a Heaviside loading history $H(t)$

$$T^{(ve)}(t) = T^{(e)} - T^{(v,1)}[\exp(-s^{(1)}t) - 1] - T^{(v,2)}[\exp(-s^{(2)}t) - 1], \quad (51)$$

which, for $t \to \infty$, becomes

$$T^{(i)} = T^{(e)} + T^{(v,1)} + T^{(v,2)}, \quad (52)$$

where superscript i denotes the inviscid limit at $t \to \infty$. The response is therefore completely characterized by the quantities $T^{(e)}$, $T^{(v,1)}$, $T^{(v,2)}$, $s^{(1)}$, $s^{(2)}$. As mentioned in Appendix C, Eq. 51 applies both for the sphere and for the half-space.

For our numerical analysis we choose three different Earth models. Model A is uniform, i.e. without elastic shell. Since the Earth is known to have a lithosphere, the uniform model may appear inappropriate. Its main purpose in the present discussion is to illuminate the modification of the response by the presence of this structural feature. In Model B the lithosphere is 100 km thick. This is a standard value for continental regions based on much previous geophysical research. A similar value has, for example, been inferred by McConnell (1968) in his analysis of glacio-isostatic rebound in Scandinavia. Model C is characterized by an enhanced lithospheric thickness of 200 km. This reflects recent estimates proposed by Peltier (1984) from his interpretation of deglaciation-induced relative-sea-level rise and polar-wander information.

In all three models the density is taken to be $\rho = 3320\,\mathrm{kgm^{-3}}$. This is considerably below the average value appropriate to the whole Earth but fairly characteristic of the material at a depth of 33 km (Bullen, 1963, pp. 232–235). Combined with $g = 9.81\,\mathrm{m\,s^{-2}}$, this reduced value insures the correct surface deflection in the inviscid limit, which, for low angular orders, is essentially independent of the elastic parameters of the lithosphere and largely determined by the near-surface density contrast. For the shear modulus of the viscoelastic mantle the value $\mu_2 = 1.45 \times 10^{11}\,\mathrm{Nm^{-2}}$ is adopted. This is the mean value for the whole Earth (e.g. Wu and Peltier, 1982, p. 442). For the lithosphere we choose $\mu_1 = 0.67 \times 10^{11}\,\mathrm{Nm^{-2}}$, which is typical of a depth of 100 km (Bullen, 1963, pp. 232–235). In all models the dynamic viscosity is $\eta_2 = 10^{22}$ P, which appears to be fairly characteristic of both the upper and the lower mantle (Cathles, 1975; Peltier, 1982).

In discussing Figs. 1–3, we will postpone the analysis of the accuracy of the half-space approximation momentarily and focus on the properties of the spherical solution.

Figure 1 shows the transfer functions for the uniform Earth model as a function of the angular order n. The quasi-linear decrease of the elastic transfer function with a slope of -1 on the double-logarithmic plot (Fig. 1a) is familiar. If the effects of gravity and sphericity are neglected, the theoretical solution is (e.g. Jeffreys, 1976, pp. 265–267)

$$T^{(e)}(k) = 1/(2\mu_1 k). \quad (53)$$

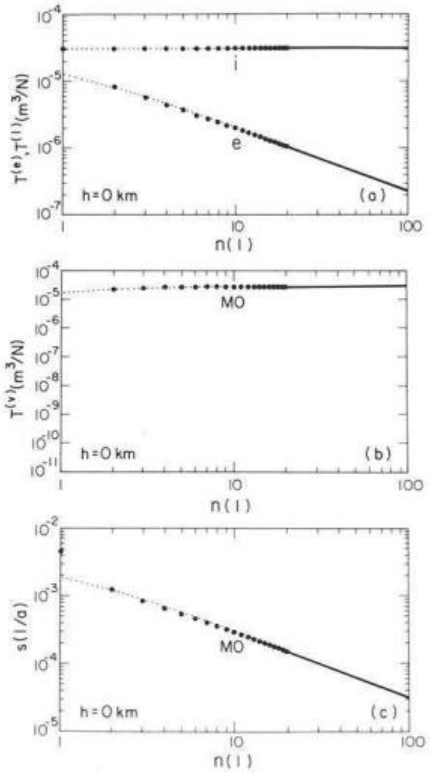

Fig. 1 a, b and c. a Elastic transfer functions $T^{(e)}$ and inviscid transfer functions $T^{(i)}$, **b** viscous transfer functions $T^{(v)}$ and **c** inverse relaxation times s as functions of angular order n for Model A. The *solid dots* refer to the spherical solution, the *dotted lines* illustrate the appropriate half-space approximations

Since Model A is uniform, the time dependence is characterized by a single relaxation mode. As Fig. 1b shows, the viscous transfer function $T^{(v)}$ increases with increasing n. This simply compensates for the reduced elastic response at large angular orders such that the inviscid transfer function $T^{(i)}$ be independent of n. The inverse relaxation time $1/s$ increases almost linearly with angular order. For a viscous half-space proportionality holds rigorously such that (Haskell, 1935)

$$1/s = 2\eta_2 k/(\rho g). \quad (54)$$

Figure 2 displays the response pattern of Model B. Since the shear modulus of the lithosphere is smaller than the mantle value, $T^{(e)}$ is enhanced at larger angular orders. The time dependence of Model B, however, differs fundamentally from that of the uniform model and is characterized by two relaxation modes. Wu and Peltier (1982) calculated the radial distribution of the shear energy for each mode and differentiated between a fundamental mantle mode M0 and a shallower fundamental lithospheric mode L0. Their terminology is adopted here. As Fig. 2b shows, the contribution of L0 is usually insignificant except around $n = 7$, where M0 and L0 are of comparable, even though reduced, amplitude. The pronounced decrease of the inviscid transfer function $T^{(i)}$ for $n > 30$ is a consequence of the attenuating effect of the lithosphere

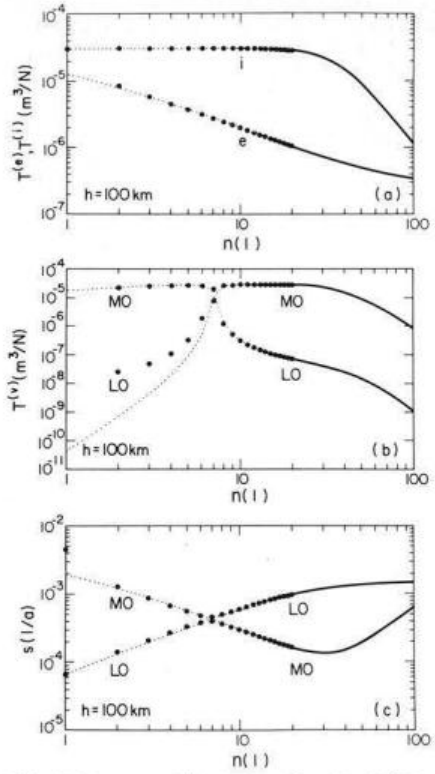

Fig. 2. Same as Fig. 1, but for Model B

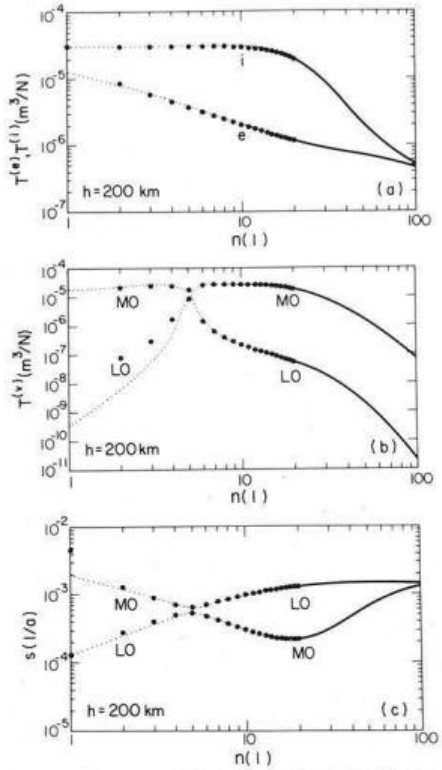

Fig. 3. Same as Fig. 1, but for Model C

at higher angular orders. If $2\pi a_1/n < h$, the lithosphere is nearly "opaque", and the response is essentially elastic. Compared to Model A, the relaxation time of the dominating mantle mode M0 is diminished at higher angular orders. This effect of the lithosphere is already known from Newtonian Earth models (e.g. McConnell, 1968).

Figure 3 summarizes the response of Model C. The general character resembles that of Model B. Since the thickness of the lithosphere is increased, the viscous contribution to the response is reduced and can be neglected for $n > 100$ (Fig. 3a and b). The inverse relaxation times $s^{(1)}$ and $s^{(2)}$, which can be shown to become identical when $n \to \infty$, have almost merged at $n = 100$.

The most interesting feature of Figs. 1–3 is the close match between spherical and half-space transfer functions down to very low angular orders. This does not, however, apply to $n = 0$, 1. At $n = 0$, incompressible spherical models appear rigid and

$$T_0^{(e)} = 0. \tag{55}$$

For the half-space models, however, we find from Eq. (40) at $k = 0$

$$T^{(e)}(0) = 1/(\rho g), \tag{56}$$

which is identical to the inviscid limit $T^{(i)}(0)$ for uniform loading. For the spherical model this is obtained from Eq. (38) for $n = 1$, where

$$T_1^{(e)} = 1/(\rho g). \tag{57}$$

Apart from that, differences are generally confined to the lithospheric mode L0 of the viscous transfer function, whose amplitude is negligible at most angular orders.

The significance of the differences mentioned above for the response to physical loads is governed by their spectral representation. If high angular orders dominate the load spectrum, the low end of the response spectrum is not sampled efficiently and the half-space approximation is expected to be adequate. For extended loads, however, the lower angular orders become increasingly important. The Laurentide ice sheet, for example, had its energy concentrated near $n = 5$ (as compared to $n = 15$ for the Fennoscandian ice sheet). An additional effect is that at low orders the Legendre series Eq. (45) will differ from its approximation Eq. (47). This is a direct consequence of the identity for Legendre functions and Bessel functions expressed by Eq. (41). If n is finite and $\theta > 0$, Eq. (41) holds only approximately.

In the following figures, the radial surface displacement $u_r(a_1)$ due to circular loads, as calculated from the spherical solution Eq. (37), is plotted and compared with the vertical surface displacement $-w(0)$ according to the half-space approximation Eq. (39). We thus compare, for $R = 800$ km and $R = 1600$ km,

$$u_r(a_1, \theta) = -\sum_{n=0}^{\infty} T_n^{(ve)} q_n P_n(\cos\theta), \tag{58}$$

with

$$-w(r', 0) = -\int_0^{\infty} T^{(ve)}(k)\, \hat{q}(k)\, k J_0(k r')\, dk, \tag{59}$$

where $T_n^{(ve)}$ and $T^{(ve)}(k)$ are given by Eq. (51) and q_n and $\hat{q}(k)$ denote the appropriate load spectra according to Eqs. (46) and (48), respectively. In each case the thickness h_0 of the load is 3 km, while its density ρ_0 is 1000 kgm^{-3}.

Figures 4 and 5 show the deflection for the uniform

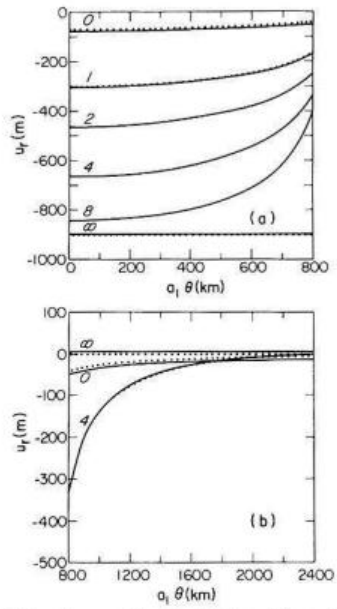

Fig. 4a and b. Radial surface displacement u_r as a function of distance $a_1\,\theta$ from the load axis for **a** the central region and **b** the peripheral region, and for several times (in units of ka) after the emplacement of the load. The *solid lines* refer to the spherical solution, the *dotted lines* illustrate the appropriate half-space approximation. Results are for Model A and $R = 800$ km

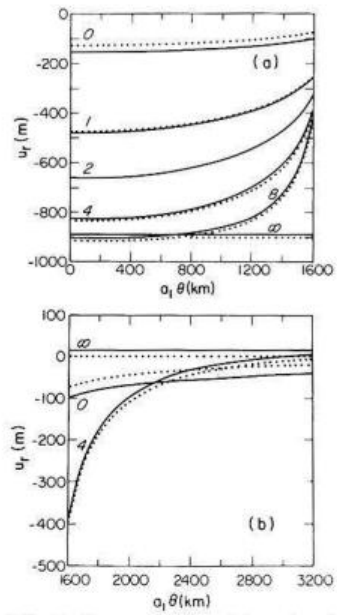

Fig. 5. Same as Fig. 4, but for Model A with $R = 1{,}600$ km

Model A. If $R = 800$ km, the half-space approximation is excellent. This also holds for $R = 1600$ km except for times directly following emplacement of the load. With increasing time, local compensation is approached. In that limit, the radius of the viscoelastic sphere is slightly increased (Figs. 4b and 5b). This reflects the conservation of volume for the incompressible model considered.

Figure 6 illustrates the response of Model B for $R = 800$ km. For this combination of lithospheric thickness and load radius, the half-space approximation is adequate. If $R = 1600$ km, the region peripheral to the

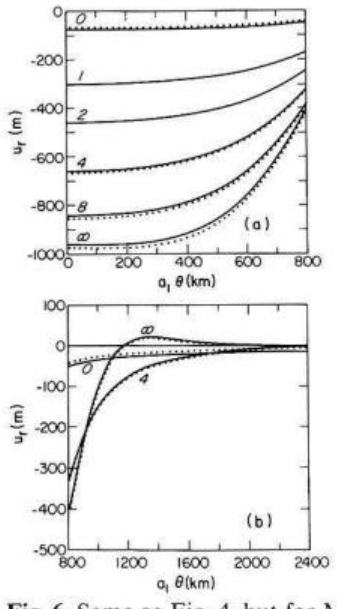

Fig. 6. Same as Fig. 4, but for Model B with $R = 800$ km

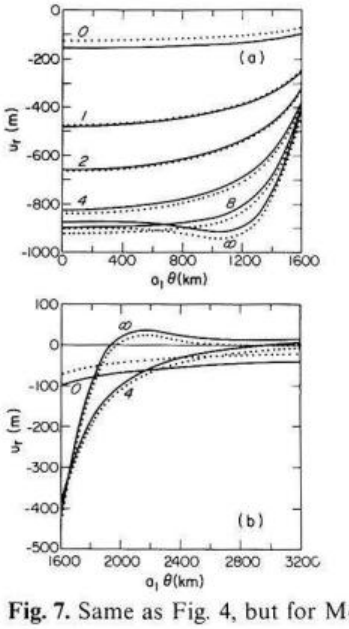

Fig. 7. Same as Fig. 4, but for Model B with $R = 1{,}600$ km

load requires special attention (Fig. 7b). Here displacements are reduced by about one order of magnitude compared to the central region below the load. This, however, results in relatively larger differences between the spherical and half-space solutions in the peripheral region. The maximum of the peripheral bulge, for example, is underestimated by about 40 per cent on the basis of half-space theory.

For Model C, which is characterized by a 200-km-thick lithosphere, the results are comparable to those of Model B. If $R = 800$ km (Fig. 8a and b), half-space solutions are again adequate. For $R = 1600$ km (Fig. 9a and b), they become marginal in the central region and inadequate in the peripheral region. As before, the maximum of the forebulge is underestimated by approximately 40 per cent.

A different aspect of our theoretical results is the sensitivity of the response to lithospheric thickness.

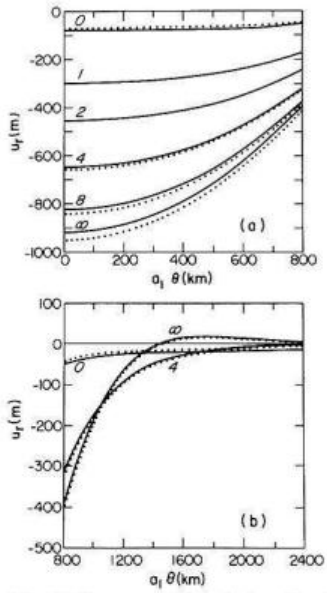

Fig. 8. Same as Fig. 4, but for Model C with $R=800$ km

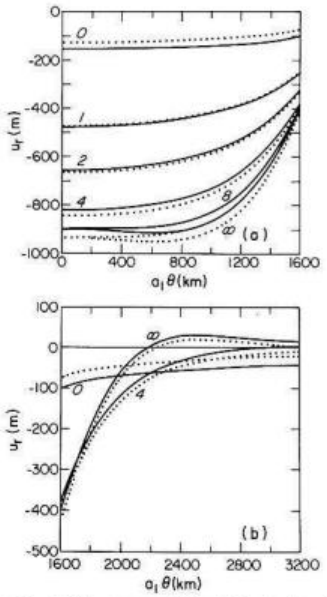

Fig. 9. Same as Fig. 4, but for Model C with $R=1{,}600$ km

Since the lithosphere becomes increasingly "transparent" with decreasing angular order of the excitation, we expect that, for $R=1600$ km, the central region below the load ($a_1\,\theta<R$) reflects this insensitivity to a certain extent. As a comparison of Figs. 5a, 7a and 9a shows, the surface deflections are quite similar for distances $a_1\,\theta<800$ km. At larger distances from the axis, and particularly at larger times, the three models differ, however, and Models B and C display an edge effect. This overshoot is already familiar from elementary thin-plate solutions for square-edged loads (e.g. Brotchie and Silvester, 1969) and has also been discussed for realistic Earth models by Wu and Peltier (1982). These authors also show that the edge effect is partially related to the load shape and vanishes if more realistic loads of parabolic or similar cross-sections are employed. As can be seen from Figs. 5b, 7b and 9b, the effect of the lithosphere becomes even more pronounced in the periphery of the load ($a_1\,\theta>R$), where the location, amplitude and shape of the bulge are closely controlled by lithospheric thickness.

If $R=800$ km, the situation is different. Near the load axis the presence of the lithosphere causes the deflection in the inviscid limit to exceed that appropriate to local compensation (Figs. 4a, 6a and 8a). By comparing Figs. 6a and 7a we realize that this behaviour is best explained by the superposition of two edge effects. As for $R=1600$ km, the excess displacement will, however, decrease for loads of smooth cross-section. The shape of the deflection curves is nevertheless distinct and reflects the effect of the lithosphere. The surface deflection in the peripheral region, on the other hand, seems less suitable for inferring lithospheric thickness. This is mainly related to the fact that, for $R=800$ km, the volume displaced by the load is small and the bulge therefore not pronounced (Figs. 4b, 6b and 8b).

Discussion and Conclusions

Prior to completion of the work discussed in this paper, the adoption of either spherical or half-space models in the interpretation of isostatic adjustment data has been based more on intuition than on rigorous analysis. For the Fennoscandian ice sheet, for example, the flat-earth approximation has been considered adequate by most authors (e.g. Haskell, 1935; McConnell, 1968). The Laurentide glaciation in Canada, on the other hand, has almost exclusively been analysed in terms of spherical Earth models (see Peltier, 1982, for a summary). A notable exception is Walcott's (1970b) interpretation. This author used a two-dimensional load representation and a flat-earth model to infer the thickness of the lithosphere from tilt data of proglacial Lake Algonquin.

Our previous analysis has confirmed the adequacy of half-space approximations when modelling deformations induced by loads comparable in scale to the Fennoscandian ice sheet. The main advantage of analytical half-space solutions is clearly that they yield much more tractable algebraic expressions compared to those required for the spherical solution. Of some consequence may also be the fact that the numerical implementation of the inverse Hankel transform, based on Simpson's rule, converges faster than the Legendre series of the associated spherical problem.

We have further shown that, for load scales comparable to that of the Laurentide ice sheet, the neglect of sphericity usually yields incorrect results. This holds particularly for the deflection in the periphery of the load. Here deformations are also sensitive to the parameters characterizing the lithosphere and may be used to infer its thickness (Peltier, 1984). This, however, renders the use of spherical models mandatory in such interpretations.

In the past, Walcott's (1970b) inference of lithospheric thickness on the basis of tilt data from Pleistocene Lake Algonquin near the margin of the Laurentide ice sheet was repeatedly questioned (e.g. Nakiboglu and Lambeck, 1982). The main objection in this criticism has been his assumption of an inviscid mantle. Here we will briefly comment on the geometry of his

model, which is characterized by a two-dimensional load resting on a flat Earth.

Using simple half-space models, it may be shown that, for load scales comparable to the Laurentide ice sheet, circular disk loads may be replaced by two-dimensional loads when calculating the deflection near the load margin (Wolf, 1984b). This, however, does not interfere with the question whether sphericity can be neglected in this case. As a cursory inspection of Walcott's theoretical curves shows, the peripheral bulge is quite small, both in amplitude and lateral extension, in his flat-earth solution. Walcott interpreted it is a short-wavelength "static bulge" superimposed on a "dynamic bulge" of larger amplitude and extension, and associated the tilt data with the former.

Quite obviously, Walcott's differentiation between two such bulges is physically not justified. From the present analysis it is further clear that the theoretical bulge increases in amplitude and lateral extent, if the appropriate spherical solution is employed (Fig. 7b). The value of approximately 100 km for the thickness of the lithosphere inferred by Walcott must therefore be viewed with some caution. Since this value is also smaller, by a factor of two, than recent estimates of lithospheric thickness for the same region (Peltier, 1984), the Lake Algonquin tilt data require re-interpretation.

A second result of our analysis has been the demonstration of the overall sensitivity of the response to lithospheric thickness for load scales comparable to the Fennoscandian ice sheet. As discussed in the previous section, this sensitivity is a simple consequence of a shift in the load spectrum to higher angular orders, at which the lithosphere appears increasingly "opaque". This is at variance with Cathles' (1975, p. 153) conclusions, who believed that the strength of the lithosphere was not sufficient to affect the uplift in the central regions of Scandinavia. McConnell (1968), on the other hand, argued that a lithosphere was required in order that the observed decrease in the relaxation time spectrum at shorter wavelengths could be explained, and inferred a value of 120 km for its thickness. McConnell's whole analysis may, however, be criticized, since it is based on the incorrect assumption that the area deformed by the glacial load essentially coincides with the area covered by the load. Considering the limitations of the past interpretations and in view of the fundamental importance of the lithosphere for several geodynamic phenomena, the Fennoscandian uplift data therefore deserve renewed attention.

Appendix A

If we are interested in the solution for a uniform elastic sphere of radius a_2 and shear modulus μ_2, the general solution of the coupled system of Eqs. (12)–(14) must yield finite field quantities at $r=0$. Then $B_n=D_n=0$ for $n=0,1,\ldots$, and the general solutions Eqs. (22)–(24), (27) and (28) simplify accordingly.

The constants A_n and C_n are determined from the boundary conditions at $r=a_2$. For generality, we allow for arbitrary pre-specified surface tractions and solve Eqs. (27) and (28) at $r=a_2$ for A_n and C_n. We obtain, since $B_n=D_n=0$,

$$2\mu_2 a_2^n (n-1)(2n^2+4n+3) A_n = -n(n^2-1)\left[\frac{\sigma_{rr}(a_2,\theta)}{P_n}+\frac{n\sigma_{r\theta}(a_2,\theta)}{\sin\theta P_n'}\right], \tag{60}$$

$$2\mu_2 a_2^{n-2}(n-1)(2n^2+4n+3) C_n = n\left[n(n+2)\frac{\sigma_{rr}(a_2,\theta)}{P_n}+\frac{(n+1)(n^2-n-3)\sigma_{r\theta}(a_2,\theta)}{\sin\theta P_n'}\right]. \tag{61}$$

Substituting for A_n and C_n in Eqs. (22) and (23) yields

$$2\mu_2(n-1)(2n^2+4n+3)u_r(r,\theta) = \left(\frac{r}{a_2}\right)^{n-1} n a_2\left\{\left[n(n+2)-(n^2-1)\left(\frac{r}{a_2}\right)^2\right]\sigma_{rr}(a_2,\theta) + \left[(n+1)(n^2-n-3)-n(n^2-1)\left(\frac{r}{a_2}\right)^2\right]\frac{P_n}{\sin\theta P_n'}\sigma_{r\theta}(a_2,\theta)\right\}, \tag{62}$$

$$2\mu_2(n-1)(2n^2+4n+3)u_\theta(r,\theta) = -\left(\frac{r}{a_2}\right)^{n-1} a_2\left\{\left[n(n+2)-(n+3)(n-1)\left(\frac{r}{a_2}\right)^2\right]\cdot\frac{\sin\theta P_n'}{P_n}\sigma_{rr}(a_2,\theta) + \left[(n+1)(n^2-n-3)-n(n+3)(n-1)\left(\frac{r}{a_2}\right)^2\right]\sigma_{r\theta}(a_2,\theta)\right\}. \tag{63}$$

If we put $r=a_2$, the required relation between the field quantities at a_2 is obtained.

Appendix B

For the constants in Eqs. (33)–(36) we obtain

$$D=[k_1' k_4+k_1 k_4'-k_2' k_6(a_2/a_1)^2-k_2 k_6'(a_2/a_1)^{-2} -k_3' k_5(a_2/a_1)^{2n+1}-k_3 k_5'(a_2/a_1)^{-(2n+1)}], \tag{64}$$

where

$$k_1=n(n+2)(2n-1)(M-1)\cdot[(2n^2+4n+3)M+2n(n+2)], \tag{65a}$$

$$k_2=(2n+1)(n^2-1)(M-1)\cdot[(2n^2+4n+3)M+2n)(n+2)], \tag{65b}$$

$$k_3=[2(n^2-1)M+2n^2+1]\cdot[(2n^2+4n+3)M+2n(n+2)], \tag{65c}$$

$$n(n+2)k_4=(2n+3)(n^2-1)^2(M-1)\cdot[(2n^2+4n+3)M+2n(n+2)], \tag{65d}$$

$$k_5=-2(n^2-1)(2n^2+4n+3)(M-1)^2, \tag{65e}$$

$$k_6=[(2n+1)M-(n-2)](n^2-1)(2n^2+4n+3)M +2n^2(n+2)(n^2+3n-1)(M-1) -[3M+2(n-1)](n+1)^2(n^2-n-3) -[(2n+1)(2n^2+n+3)+3(n+3)(n^2-1)](n+1)M, \tag{65f}$$

$$k_1'=n^2(n+2)^2(2n-1), \tag{66a}$$

$$k_2'=n(n+1)(2n+1)[(n-1)(n+2)+F_1], \tag{66b}$$

$$k_3'=-n[(n+2)(2n^2+1)-(n+1)(2n+1)F_1], \tag{66c}$$

$$k'_4=(n^2-1)^2(2n+3), \tag{66 d}$$

$$k'_5=(n+1)[(n-1)(2n^2+4n+3)+n(2n+1)F_1], \tag{66 e}$$

$$k'_6=(n+1)(n^2-1)(n^2-n-3)+n^2(n+2)\cdot(n^2+3n-1)-n(n+1)(2n+1)F_1. \tag{66 f}$$

Here we have used $M=\mu_2/\mu_1$ and $F_1=\rho g a_1/(2\mu_1)$.

Appendix C

In the following, $T^{(e)}$ may be interpreted either as the elastic transfer function $T_n^{(e)}$ according to the spherical solution Eq. (38) or the half-space approximation $T^{(e)}(k)$ according to Eq. (40). In either case, $T^{(e)}$ can be written in the form

$$T^{(e)}=\frac{e_0+e_1 M+e_2 M^2}{d_0+d_1 M+d_2 M^2}, \tag{67}$$

where $M=\mu_2/\mu_1$. The coefficients are complicated expressions of the model parameters. With $M\to M(s)=\mu_2(s)/\mu_1$, where $\mu_2(s)$ is given by Eq. (50), Eq. (67) can also be interpreted as the Laplace transform

$$\tilde{T}^{(ve)}(s)=\frac{E_0+E_1 s+E_2 s^2}{D_0+D_1 s+D_2 s^2} \tag{68}$$

of the transfer function $T^{(ve)}(t)$ appropriate to the associated viscoelastic solution for an impulsive surface load $q\delta(t)$ (see Peltier, 1974, for details). Equation (68) is written in terms of powers of the Laplace transform variable s. The upper-case coefficients of Eq. (68) are easily expressed in terms of the lower-case coefficients of Eq. (67) and $M(s)$. The transform $\tilde{T}^{(ve)}(s)$ of the viscoelastic transfer function may be split into an elastic portion $T^{(e)}$ and a viscous portion $\tilde{V}(s)$, i.e.

$$\tilde{T}^{(ve)}(s)=T^{(e)}+\tilde{V}(s), \tag{69}$$

where

$$T^{(e)}=\lim_{s\to\infty}\tilde{T}^{(ve)}(s). \tag{70}$$

$T^{(e)}$ is given by Eq. (38) or Eq. (40) and interpreted as the Laplace transform of the instantaneous elastic response of the viscoelastic system to the impulsive load applied at $t=0$. The transform $\tilde{V}(s)$ of the viscous portion can be cast into the form

$$\tilde{V}(s)=T^{(v,1)}\frac{s^{(1)}}{s+s^{(1)}}+T^{(v,2)}\frac{s^{(2)}}{s+s^{(2)}}, \tag{71}$$

where $T^{(v,1)}$, $T^{(v,2)}$ and $s^{(1)}$, $s^{(2)}$ are given in terms of the coefficients in Eq. (68). Implementing the inverse Laplace transform yields

$$T^{(ve)}(t)=T^{(e)}\delta(t)+T^{(v,1)}s^{(1)}\exp(-s^{(1)}t)+T^{(v,2)}s^{(2)}\exp(-s^{(2)}t). \tag{72}$$

This is the system's impulse response. The response to a Heaviside loading history follows from convolving it with the impulse response. From Eq. (72) we obtain for $t\geqq 0$

$$T^{(ve)}(t)=T^{(e)}-T^{(v,1)}[\exp(-s^{(1)}t)-1]-T^{(v,2)}[\exp(-s^{(2)}t)-1]. \tag{73}$$

Acknowledgements. This research was financially supported by a Natural Sciences and Engineering Research Council of Canada Postgraduate Scholarship. Special thanks are due to Richard Peltier for stimulating discussions and to Khader Khan for drafting the figures.

References

Brotchie, J.F., Silvester, R.: On crustal flexure. J. Geophys. Res. **74**, 6240–5252, 1969

Bullen, K.E.: An introduction to the theory of seismology, 3rd edn. Cambridge: Cambridge University Press 1963

Cathles, L.M.: The viscosity of the Earth's mantle. Princeton: Princeton University Press 1975

Crittenden, M.D. jr.: Effective viscosity of the Earth derived from isostatic loading of Pleistocene Lake Bonneville. J. Geophys. Res. **68**, 5517–5530, 1963

Dragoni, M., Yuen, D.A., Boschi, E.: Global postseismic deformation in a stratified viscoelastic Earth: effects on Chandler wobble excitation. J. Geophys. Res. **88**, 2240–2250, 1983

Haskell, N.A.: The motion of a viscous fluid under a surface load. Physics **6**, 265–269, 1935

Jeffreys, H.: The Earth, 6th edn. New York: Cambridge University Press 1976

Lebedev, N.N.: Special functions and their applications. New York: Dover 1972

Love, A.E.H.: Some problems of geodynamics. Cambridge: Cambridge University Press 1911

Love, A.E.H.: A treatise on the mathematical theory of elasticity, 4th edn. Cambridge: Cambridge University Press 1927

McConnell, R.K.: Viscosity of the mantle from relaxation time spectra of isostatic adjustment. J. Geophys. Res. **73**, 7089–7105, 1968

Nakiboglu, S.M., Lambeck, K.: A study of the Earth's response to surface loading with application to Lake Bonneville. Geophys. J. R. Astron. Soc. **70**, 577–620, 1982

Peltier, W.R.: The impulse response of a Maxwell Earth. Rev. Geophys. Space Phys. **12**, 649–669, 1974

Peltier, W.R.: Ice sheets, oceans, and the Earth's shape. In: Earth rheology, isostasy, and eustasy, N.-A. Moerner, ed.: pp. 45–63. New York: Wiley 1980

Peltier, W.R.: Dynamics of the ice age Earth. Adv. Geophys. **24**, 1–146, 1982

Peltier, W.R.: The thickness of the continental lithosphere. J. Geophys. Res. 1984 (in press)

Slichter, L.B., Caputo, M.: Deformation of an Earth model by surface pressures. J. Geophys. Res. **65**, 4151–4156, 1960

Sneddon, I.A.: Fourier transforms. New York: McGraw-Hill 1951

Walcott, R.I.: Flexural rigidity, thickness, and viscosity of the lithosphere. J. Geophys. Res. **75**, 3941–3954, 1970 a

Walcott, R.I.: Isostatic response to loading of the crust in Canada. Can. J. Earth Sci. **7**, 716–727, 1970 b

Watson, G.N.: A treatise on the theory of Bessel functions, 2nd edn. Cambridge: Cambridge University Press 1944

Wolf, D.: Thick plate flexure re-examined. Geophys. J. R. Astron. Soc. 1984 a (in press)

Wolf, D.: On the relation between two-dimensional and axisymmetric loads in plate flexure problems. J. Geophys. **54**, 232–235, 1984

Wu, P., Peltier, W.R.: Viscous gravitational relaxation. Geophys. J. R. Astron. Soc. **70**, 435–485, 1982

Received February 1, 1984; Revised version July 10, 1984
Accepted July 11, 1984